IFASD 2015
International Forum
on Aeroelasticity and Structural Dynamics
June 28 — July 02, 2015 ▲ Saint Petersburg, Russia

PASSIVE CONTROL OF TRANSONIC BUFFET ONSET ON A HALF WING–BODY CONFIGURATION

S. Timme[1] **and F. Sartor**[1]

[1]School of Engineering, University of Liverpool
Liverpool L69 3GH, United Kingdom
Sebastian.Timme@liverpool.ac.uk

Keywords: Shock Buffet Onset, Transonic Flow, Half Wing-Body Configuration, Computational Fluid Dynamics, Mechanical Vortex Generators, DLR-TAU Code

Abstract: This paper presents a numerical study of the transonic flow over a half wing-body configuration representative of a large civil aircraft. Results indicate the presence of shock-wave oscillations that induce unsteady loads and can cause serious damage to the aircraft. The work focusses on the onset of the buffet unsteadiness and its control by means of passive control devices. Reynolds-averaged Navier-Stokes simulations using the Spalart-Allmaras turbulence model are considered with vortex generators fully resolved and included into the computational grid. It is shown how mechanical vortex generators modify the flow field downstream of the shock location by suppressing separation and are thus able to delay buffet onset.

1 INTRODUCTION

At cruise conditions, the flow around the wing of an aircraft is characterised by the presence of shock waves interacting with the boundary layers to cause separation. Large-scale shock movements, known as buffet, can occur [1]. While the unsteadiness is self-sustained, the resulting unsteady aerodynamic loads can excite the wing structure. As a consequence shock buffet limits the flight envelope of civil aircraft in the transonic range. Understanding such flow physics is thus of outstanding importance to aircraft designers and it has been been studied intensively by means of experimental [2,3] and numerical [4,5] investigations. The unsteadiness can be observed in both two- and three-dimensional configurations. In contrast to the two-dimensional aerofoil case with harmonic shock motions at a distinct frequency, it is often reported that shock buffet on swept wing configurations is characterised by smaller chord-wise shock movements with a larger frequency band [6]. Results of a recent study on a half wing-body configuration indicate that the onset of shock buffet can occur at a distinct frequency, while broadband unsteadiness develops with increasing distance from the onset conditions [7].

Much work has been done aiming to control and delay the onset of the buffet unsteadiness. Different approaches have been followed recently considering both active and passive control devices [8,9]. Active control devices, such as fluidic vortex generators or actuated trailing edge devices, are actively developed and have the potential to be used widely in future applications. To date however, only few investigations have proven their ability of effectively suppressing the shock unsteadiness in transonic configurations [10]. Among passive control devices, mechanical vortex generators are often used due to their simplicity

and success in other aerodynamic situations. The induced vortex downstream of the device increases the mixing between the higher momentum outer and lower momentum near-wall flow, energising the boundary layer to become less prone to separation [11, 12]. Most often, vortex generators are small vanes acting as lifting surfaces with their trailing vortex flowing over the wing. Numerical simulations over a two-dimensional profile have shown that buffet can be suppressed using such devices; the level of pressure fluctuations in the buffet region is reduced and the averaged shock wave position is pushed downstream, resulting in increased total lift [13]. In three-dimensional cases, vortex generators usually form co- or counter-rotating arrays distributed along the span. In recent studies, it was observed that the flow behaviour is significantly modified at higher angles of attack leading to higher lift coefficient values [14, 15].

In computational aerodynamics, two approaches are commonly used to simulate the flow structures induced by mechanical vortex generators; either by explicitly meshing the geometry or by adding source terms to the governing equations to model the effect of the devices. Simulating the entire control device requires considerable effort in preparation of appropriate geometry and during mesh generation. It is the most common method but must be applied with care since the results can show dependency on the numerical approach and turbulence model used [14]. To avoid high-demanding simulations, a number of reduced-order models have been proposed to represent the influence of vortex generators on the flow without fully resolving all geometric details. The available approaches can be divided into two categories; modelling the vortex generator and modelling the induced vortex. In the first approach, additional forcing terms are added to the flow equations in order to align the flow where the vortex generator would be [16–18]. In the second approach, the vortex is modelled independently of the underlying geometry by superposition of the base flow with the velocity profile corresponding to the induced vortex. This is most useful when details of the flow local to the vortex generator are less important than the downstream impact [19, 20]. A more detailed review and comparison of these methods is presented in [21].

In Section 2 the test case and numerical setup of the simulations using the DLR-TAU code are outlined. Results of steady-state and time-accurate simulations are discussed in Section 3 to investigate the characteristics and control of shock buffet using mechanical vortex generators.

2 NUMERICAL SETUP

Test Case

The chosen test case is a half wing-body configuration, shown in figure 1, representative of a large civil aircraft. The model, referred to as RBC12 in the current study, is the refurbishment of a model studied previously to investigate the effect of nacelle installation on an aircraft wing [22]. The model has a span of 1.10 m, while the aerodynamic mean chord is about 0.279 m. The local chord lengths corresponding to the centre line and wing tip are 0.592 m and 0.099 m, respectively. The wing is twisted, tapered and has a constant sweep angle of 25 deg. The trailing edge thickness of the aerofoil varies between 0.2 and 0.8 mm, depending on the span-wise location. Recently, the RBC12 configuration has been tested in the transonic wind tunnel facility of the Aircraft Research Association in the United Kingdom.

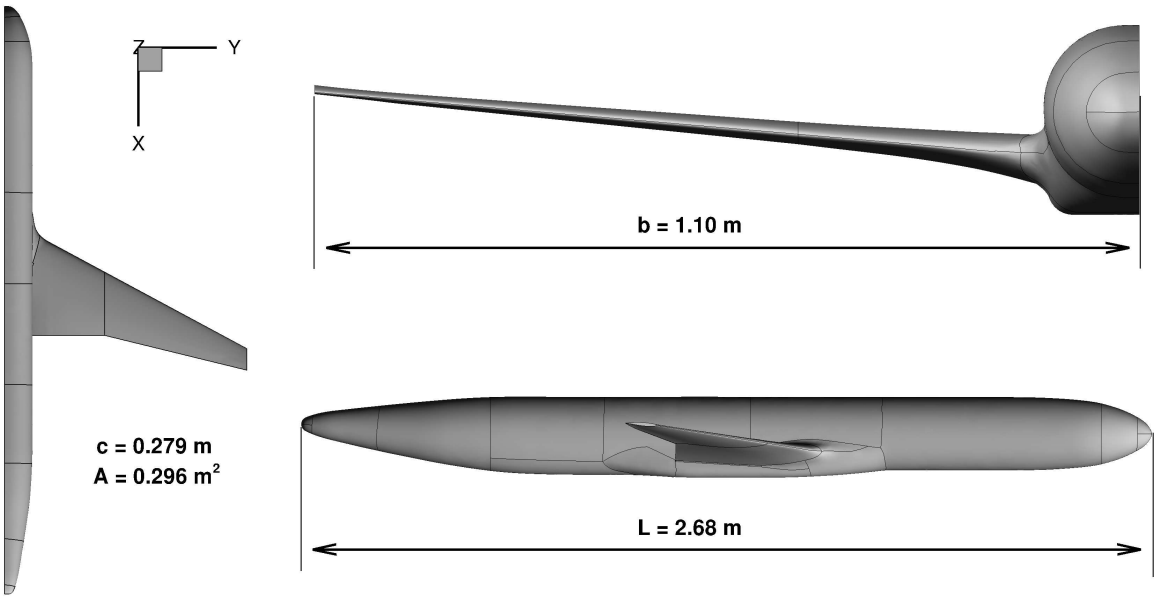

Figure 1: Top, front and side views of RBC12 half wing-body configuration.

The mechanical control device installed on the RBC12 wing during the wind tunnel tests was an array of 30 vortex generators located at 32% of local chord between 64% and 91% of the span. The spacing between individual vortex generators is 10 mm giving a span-wise spacing to height ratio of 7.7. The setting angle is at 17 deg with respect to the fuselage centre line, toed in and co-rotating. The vortex generators have a height of 1.3 mm, a bottom length of 5 mm with a taper ratio of 0.6, an aspect ratio of 1.3 and 60 deg sweep. The height is approximately equal to the boundary layer thickness just upstream of the shock location at buffet onset at Mach 0.8. The design and distribution was chosen to allow the maximum separation control as focus of the experiment.

The flow conditions are imposed to reproduce the aerodynamic field related to the wind tunnel test campaign. The Mach number discussed in the current study is 0.8, while the Reynolds number (based on the aerodynamic mean chord) is 3.75 million. The reference temperature is 266.5 K and the reference pressure is 66 kPa. Laminar to turbulent transition is imposed on the lower surface at about 5% of local chord, while on the upper surface this is at about 10% outboard of the crank and at 15% inboard. Far-field conditions are imposed at a distance corresponding to 25 times the span of the model (around 90 aerodynamic mean chord). Symmetry boundary conditions were applied along the centre plane. Several angles of attack are discussed varying between 0.0 and 4.2 deg.

DLR–TAU Solver Settings

The simulations were performed using the unstructured finite volume solver TAU, developed by the German Aerospace Center (DLR) and widely used in the European aerospace sector. The second-order central scheme with scalar dissipation was used for the convective fluxes of the mean flow equations, while a first-order Roe scheme was employed for the convective terms of the Spalart-Allmaras turbulence model [23]. Gradients of the flow variables, used for the diffusive and source terms, are calculated using the Green-Gauss theorem. Convergence of the flow equations is accelerated using local time stepping and an implicit Backward Euler solver with an LU-SGS (Lower-Upper Symmetric Gauss-Seidel)

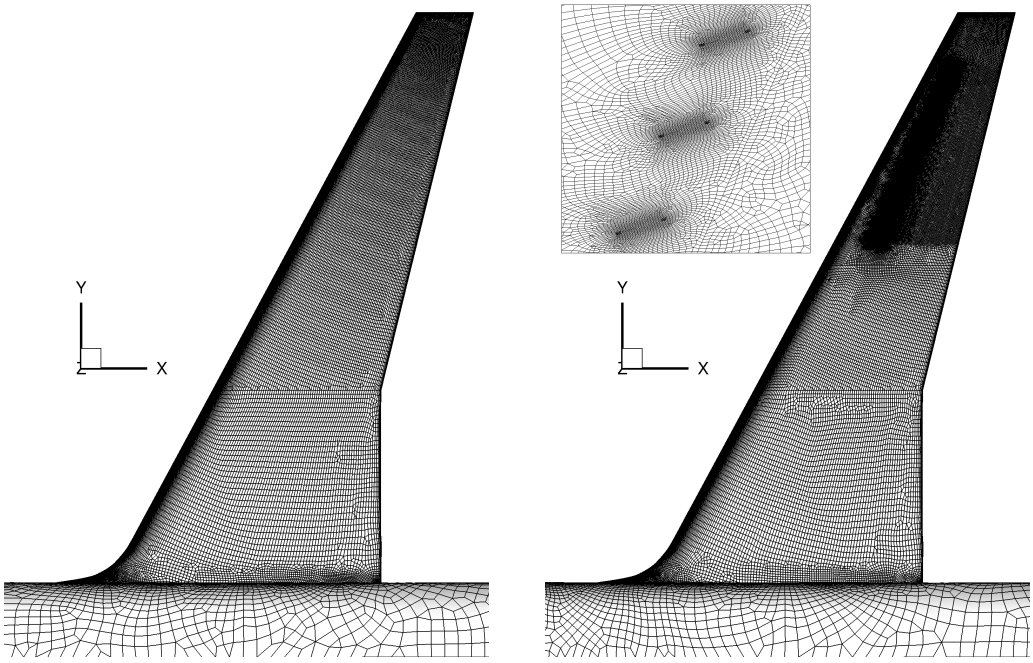

(a) Baseline with 2.7 million points (b) Refined with 6.1 million points

Figure 2: Surface mesh of baseline version and refined version with vortex generators.

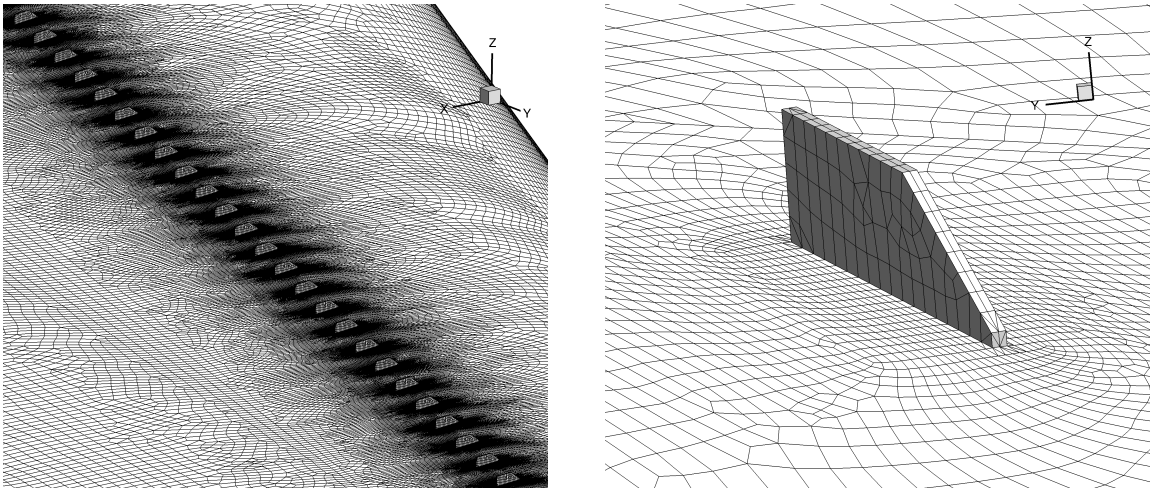

(a) Array of vortex generators (b) Individual vortex generator

Figure 3: Close-up views of vortex generators.

scheme. For time-accurate computations the standard dual time stepping approach is employed. Multigrid is not applied in the current study.

The steady-state simulations are iterated until the density residual has dropped about eight orders of magnitude. For unsteady simulations a more flexible approach is applied to account for the locally varying flow complexity during a buffet cycle. A dynamic Cauchy convergence criterion with the drag coefficient as control variable is used guaranteeing that the relative error over the last 20 iterations is less than 10^{-8}. Regardless of the Cauchy convergence control, a minimum and maximum number of 60 and 150 iterations, respectively, is enforced and chosen based on previous parametric tests. The time step size of the unsteady simulations is fixed at 2 μs.

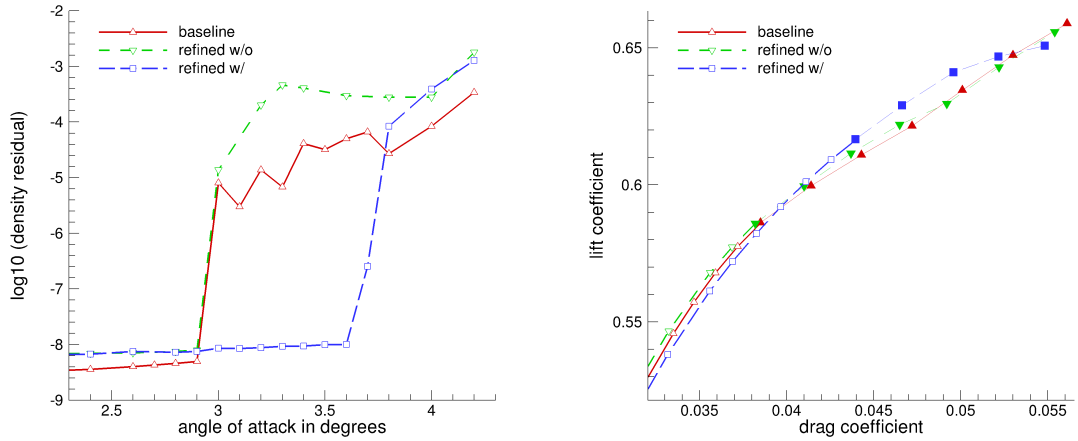

(a) Convergence of density residual

(b) Drag polars

Figure 4: Convergence of density residual normalised by initial residual and drag polars comparing results for all three meshes.

Solar Meshes

Results for three unstructured meshes are presented herein, including two meshes for the clean configuration without control devices and one for the configuration with vortex generators. The vortex generators are fully resolved using a body-fitted mesh. All meshes were produced using the Solar grid generator [24] following industry accepted guidelines. The first mesh, referred to as baseline, is used as a reference case as it has previously been used to analyse shock buffet in [7,25]. It is composed of 2.7 million points with 4.7 million volume and 97,000 surface elements. The second clean mesh is refined in the outer wing sections where the vortex generators are located. It is composed of 5.9 million points with 9.1 million volume and 199,000 surface elements. These two meshes are included to understand the differences in the flow field due to the spatial refinement. The mesh of the configuration with control devices corresponds in spatial resolution to the second mesh for the clean configuration except that now the vortex generators are included and fully resolved. There are 6.1 million points with 9.4 million volume and 204,000 surface elements. The surface grid spacing of the baseline version as well as the refined version with vortex generators can be seen in figure 2. A more detailed view of the array of vortex generators can be found in figure 3.

3 RESULTS

First results of the investigation at the freestream Mach number of 0.8 and various angles of attack are now discussed. Steady-state simulations are analysed to understand how the control devices change the characteristics of the flow field in order to delay the buffet onset. Then, unsteady simulations are presented. The focus of the discussion is on the configuration with vortex generators, while the clean wing results are also presented as reference. Clean wing data have previously been investigated in [7, 25]. Results for the baseline grid are included for comparison to confirm that changes to the buffet onset are not due to the grid refinement.

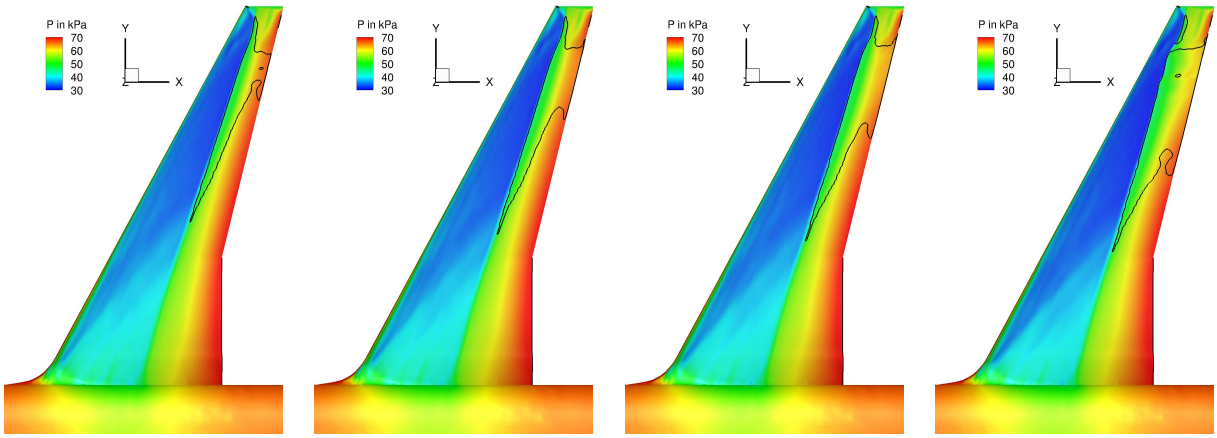

(a) 2.8 deg (b) 2.9 deg (c) 3.0 deg (d) 3.1 deg

Figure 5: Surface pressure distribution and separation line following steady-state simulation for clean wing at different angles of attack.

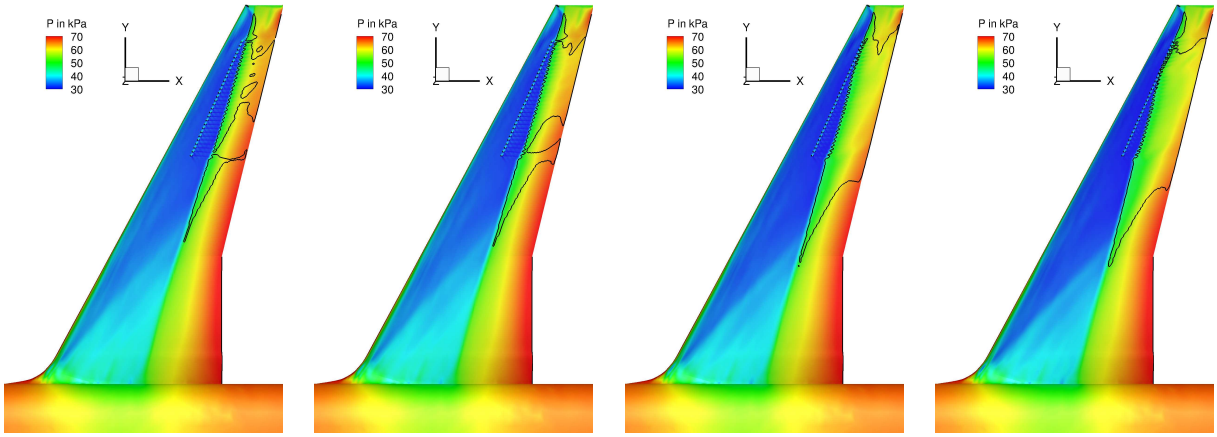

(a) 3.0 deg (b) 3.1 deg (c) 3.4 deg (d) 3.6 deg

Figure 6: Surface pressure distribution and separation line following steady-state simulation for wing with vortex generators at different angles of attack.

Steady–State Simulations

The convergence of the steady-state simulations as well as drag polars are shown in figure 4. Both the baseline grid and the two refined grids with and without vortex generators are included. Figure 4a gives the density residual normalised by the initial value. Close agreement between the two grids for the clean wing configuration is observed, thus the grid dependence is low. The simulations fail to converge at about 3.0 deg angle of attack, which, in the previous clean wing studies, was indeed found to be just below the buffet onset. While it is noted that the convergence for increasing angles of attack, beyond the clean buffet onset, slows down using the same parameter settings, the configuration with control converges until about 3.6 deg. From the unsteady simulations discussed in the next section, this angle of attack coincides with the development of unsteadiness as well. Thus, for the results presented, non-converging steady-state simulations indicate the onset of shock buffet to within 0.1 deg with respect to time-accurate simulations.

Figure 4b shows details of the drag polars below and above the buffet onset. Note that for the unsteady points on the polar, the averaged values of time-accurate simulations

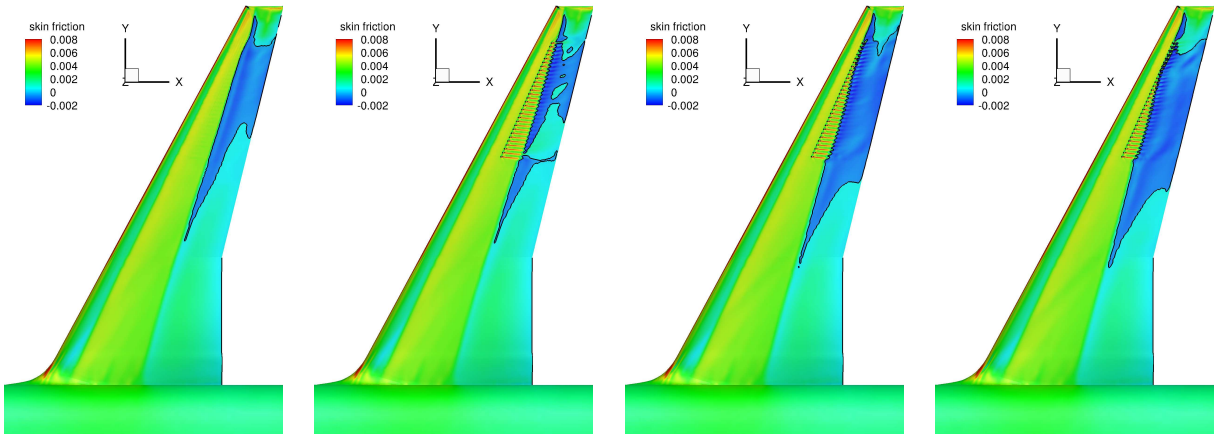

(a) clean at 3.0 deg (b) with vg at 3.0 deg (c) with vg at 3.4 deg (d) with vg at 3.6 deg

Figure 7: Skin friction coefficient and separation line following steady-state simulation for clean wing and wing with vortex generators (vg) at different angles of attack.

are included instead. These are highlighted by bigger symbols. In the region below buffet onset on the clean configuration, an increased drag of the configuration with vortex generators is observed. Beyond the buffet onset the averaged drag values for the same lift coefficient are lower compared to the uncontrolled configuration.

Figures 5 and 6 show the surface pressure distribution around the buffet onset points both for the clean configuration and the configuration with control. The separated zone is highlighted by the solid black line to indicate where the skin friction coefficient changes sign. The clean wing results in figure 5 are presented using the refined mesh and the agreement compared with previous results on the baseline grid is excellent [7]. On the inner section of the wing, the local Mach number is relatively small and the pressure jump caused by the weak shock is smeared across the profile. When moving towards the wing tip, the pressure jump across the shock wave is more pronounced. The shock foot moves upstream on the wing surface with increasing angle of attack, and a shock-induced separation is then obtained once the local Mach number exceeds a given threshold. For small angle of attack, the separated zone is visible only outboard of the crank with the reattachment line located on the wing surface. With increasing angle of attack however, the recirculation zone moves towards the trailing edge and increases in size. Even though the separated region extends from the shock foot to the trailing edge, shock buffet is only observed once the separated region splits, which is obtained for angles of attack exceeding 3.0 to 3.1 deg.

Comparing the clean wing results around buffet onset, i.e. between 3.0 and 3.1 deg angle of attack, with figure 6 for the configuration with control, the flow field downstream of the vortex generators is a lot more complex with the recirculation region having several patches of attached flow. Also, the shock foot is located slightly more downstream. With increasing angle of attack, the separated zone increases in size and again becomes continuous, until it breaks up near the wing tip region just below the buffet onset for the controlled configuration, similar to the clean case. The shock moves upstream and begins to align with the array of vortex generators. The pronounced pressure drop in the trailing edge region, which is occasionally used as indiactor for buffet onset, starting at subcritical angles of attack of about 3.3 to 3.4 deg is interesting to note.

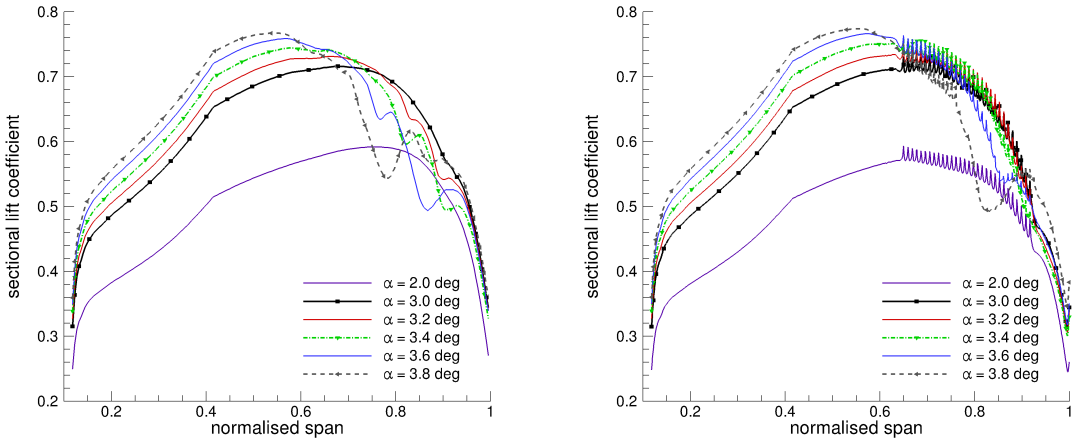

(a) clean configuration

(b) with vortex generators

Figure 8: Sectional lift coefficient comparing configurations with and without vortex generators at different angles of attack.

The corresponding skin friction distribution is presented in figure 7 for a few angles of attack. The transition line near the leading edge as well as the shock foot are clearly visible. In addition, the effect of the vortex generators becomes obvious; the boundary layer downstream of the devices is more energised as seen from higher skin friction values.

Next we look at the sectional lift coefficient along the span of the wing to discuss the presence of unsteadiness and its position. The sectional lift coefficient is computed by integrating the normal component of the steady-state pressure coefficient along the chord. The results for the clean case are presented in figure 8a. The presence of the crank can be noticed by a small discontinuity at 42% of the span. Inboard of the crank and in its vicinity up to about 50% of the span, the sectional lift coefficients keep steadily increasing with the angle of attack. Focussing on the region close to the wing tip above 70% span on the other hand, the pressure loss due to the shock-induced separated zone causes an abrupt drop in the sectional lift coefficient beyond 3.0 deg angle of attack with the separation moving inboard. It should be kept in mind however that strictly an unsteady approach is required for non-converging steady-state simulations.

In figure 8b the location of the 30 vortex generators can clearly be seen from the serrated appearance of the lift curves. The lower pressure at the vortex core is projected onto the wing surface to locally increase the lift coefficient. For angles of attack above the buffet onset of the clean configuration and below that of the controlled case, the sectional lift distributions are rather similar, particularly above 70% span. A pressure drop similar to the clean wing case is then observed at buffet onset and above.

Time–Accurate Simulations

Time histories of the lift and drag coefficients for both the clean and controlled configurations are shown in figures 9 and 10. For the clean wing data, also the corresponding histories of the baseline mesh are included for comparison. Good agreement in terms of both mean value and standard deviation can be observed confirming the rather low grid dependence. Close to buffet onset, the amplitudes of the signals around the mean

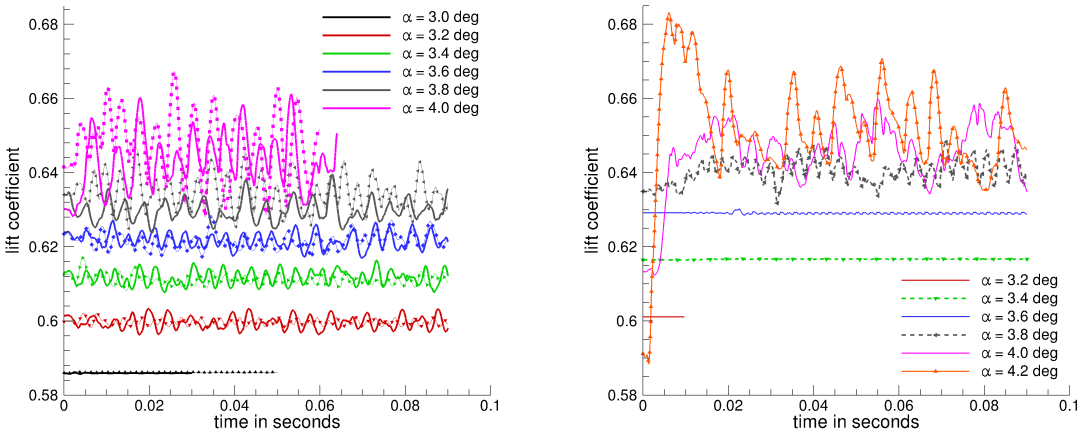

(a) clean configuration (b) with vortex generators

Figure 9: Time histories of lift coefficient at different angles of attack comparing baseline version and refined grids with and without vortex generators. Symbols in the figure to the left represent baseline grid.

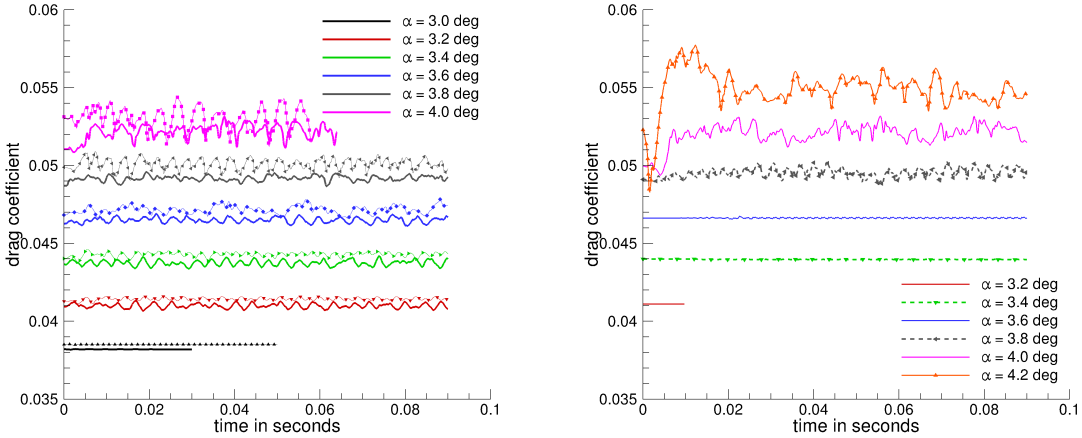

(a) clean configuration (b) with vortex generators

Figure 10: Time histories of drag coefficient at different angles of attack comparing baseline grid and refined grids with and without vortex generators. Symbols in the figure to the left represent baseline grid.

values are low, while increasing with higher angles of attack. For the configuration with control, it is interesting to note that there are high frequency, low amplitude oscillations for angles of attack of 3.4 and 3.6 deg even though the steady-state simulations converge, indeed at a lower rate. As can be seen below in figure 14a for 3.6 deg angle of attack, the unsteadiness is centred around the vortex generators. Similar behaviour is found for the case at 3.4 deg. Once the effect of the control devices of suppressing shock buffet is overcome, large amplitude unsteadiness can be seen.

In terms of frequency content, the power spectral density of the lift coefficient only is provided in figure 11. The corresponding power spectral density of the drag coefficient is very similar and thus not included. An autoregressive spectral estimator [26] following

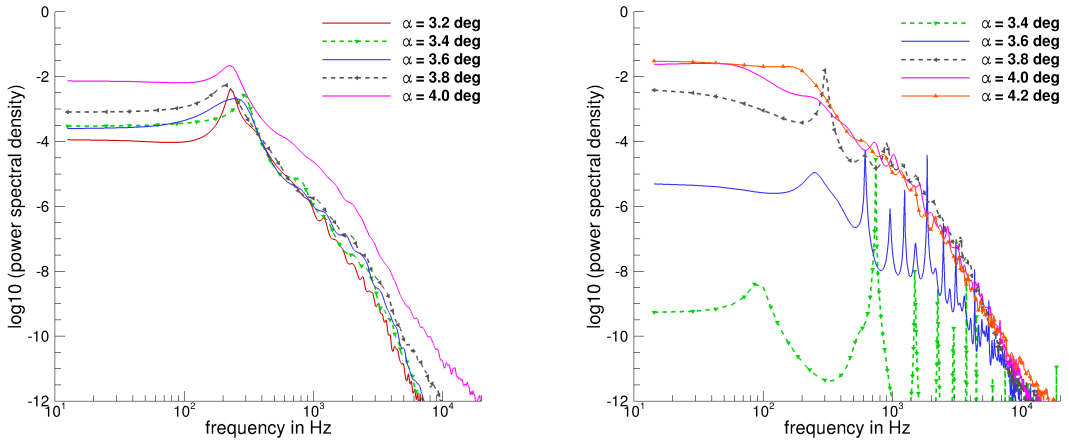

(a) clean configuration (b) with vortex generators

Figure 11: Power spectral density of lift coefficient.

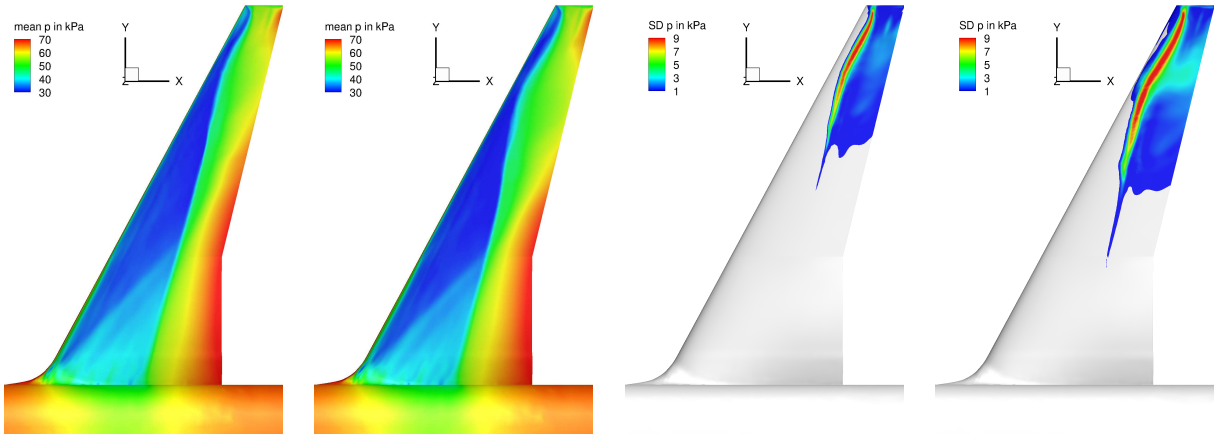

(a) mean at 3.6 deg (b) mean at 4.0 deg (c) SD at 3.6 deg (d) SD at 4.0 deg

Figure 12: Mean surface pressure distribution and standard deviation (SD) following time-accurate simulations for clean wing at different angles of attack.

Burg's method [27] is used rather than the usual Fast Fourier Transform. Following a parametric study, the order of Burg's method is set to 2000. For the clean configuration, there is a more pronounced peak centred at about 200 to 300 Hz close to buffet onset. With increasing angle of attack, this peak becomes more broadband as is commonly reported for the shock buffet instability. For the configuration with control, the low-amplitude, high-frequency unsteadiness observed in the time histories is also found in the power spectral density for angles of attack of 3.4 and 3.6 deg at 740 and 610 Hz, respectively. Interestingly, for 3.6 deg angle of attack, there is a broadband, low intensity peak centred between 200 and 300 Hz which seems to corresponds to the suppressed buffet instability. This lower frequency peak first becomes rather dominant at 3.8 deg and then broadband for angles of attack above that, similar to the case without control.

To have a better idea of the spatial distribution of the unsteadiness, we present mean values and standard deviation of the surface pressure distribution, readily available in the DLR-TAU code, in figures 12 through 14. Clean wing results as shown in figure 12 are

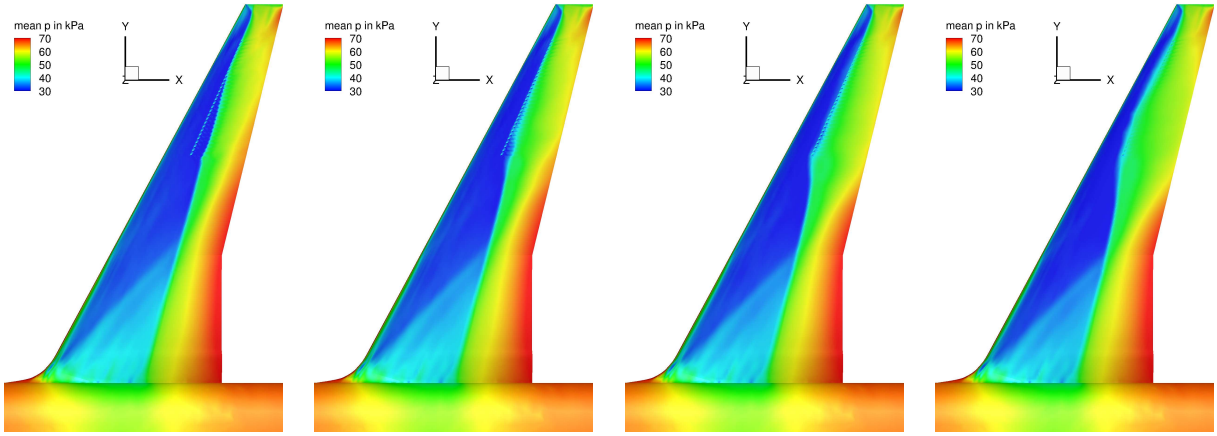

(a) 3.6 deg (b) 3.8 deg (c) 4.0 deg (d) 4.2 deg

Figure 13: Mean surface pressure distribution following time-accurate simulation for wing with vortex generators at different angles of attack.

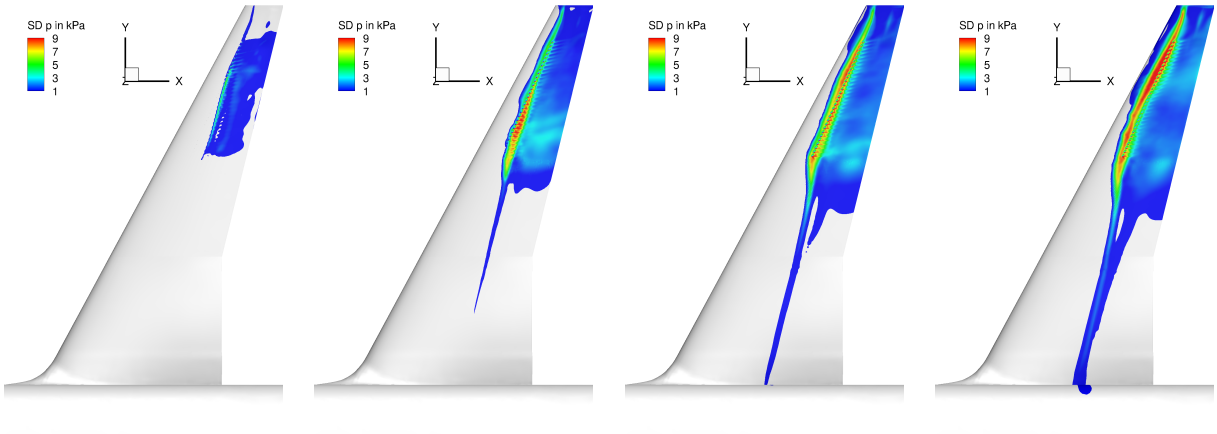

(a) 3.6 deg (b) 3.8 deg (c) 4.0 deg (d) 4.2 deg

Figure 14: Standard deviation of surface pressure distribution following time-accurate simulation for wing with vortex generators at different angles of attack.

very similar to the results presented in [7]. Looking at sequences of instantaneous pressure distributions, which are not included herein, it can be seen that a curved shock wave of almost sinusoidal shape keeps moving continuously towards the wing tip constituting the instability. Such behaviour was also observed in the experimental investigation analysing data from dynamic pressure sensitive paint. The highest intensity of the pressure standard deviation corresponds to the mean location of the curved shock foot, as should be expected, while downstream of which, in the separated zone, high levels of unsteadiness are observed as well. With increasing angle of attack, the stream-wise and span-wise extent of the shock motion increases.

Corresponding surface pressure values for the configuration with control are shown in figures 13 and 14. It is very interesting to observe that the mean shock positions, as can also be seen in the standard deviation plots, seem to align distinctively with the array of vortex generators starting from the wing tip for lower angles of attack and then moving inboard. In addition, the levels of pressure standard deviation are reduced compared to the clean configuration.

4 CONCLUSIONS

The current paper presents a numerical study to investigate the effect of mechanical vortex generators to delay the onset of transonic shock buffet on a half wing-body configuration. Using the DLR-TAU code, the Reynolds-averaged Navier-Stokes equations coupled with the Spalart-Allmaras turbulence model are chosen as aerodynamic model. The vortex generators are fully resolved using a body-fitted mesh. Steady and time-accurate simulation at a freestream Mach number of 0.8 and various angles of attack are conducted comparing results from a clean configuration without control and the equivalent version with control devices installed.

Steady-state results indicate that the vortex generators delay the buffet onset by about half a degree in angle of attack by modifying the separated zone downstream of the shock wave. The effect of the vortex generators via the induced vortex on the flow field is clearly visible. Failure to converge the steady-state simulations is a fair predictor to judge the buffet onset, while unsteady simulations confirm the results. Unsteady simulations for angles of attack beyond the buffet onset indicate that the mean shock position and high intensity pressure fluctuations align with the array of vortex generators starting near the wing tip close to buffet onset and then moving inboard. Time histories and frequency content of the integrated lift and drag coefficients reveal high frequency oscillations even below buffet onset in addition to a typical frequency of the suppressed buffet instability. Once the effect of the vortex generators is overcome, broadband frequency content at about 200 to 300 Hz related to shock buffet is observed.

Further studies will investigate different turbulence models and finer-resolved meshes, particularly near the vortex generators. In addition, detailed comparisons with recent wind tunnel tests will be accomplished.

5 ACKNOWLEDGMENTS

The authors wish to acknowledge Simon Lawson and Marco Hahn from Aircraft Research Association for providing the meshes. The research leading to these results has received funding from the European Union's Seventh Framework Programme (FP7/2007-2013) for the Clean Sky Joint Technology Initiative under grant agreement n° 336948.

6 REFERENCES

[1] Lee, B. H. K. (2001). Self-sustained shock oscillations on airfoils at transonic speeds. *Progress in Aerospace Sciences*, 37(2), 147–196.

[2] McDevitt, J. B., Levy, J. L. L., and Deiwert, G. S. (1976). Transonic flow about a thick circular-arc airfoil. *AIAA Journal*, 14(5), 606–613.

[3] Jacquin, L., Molton, P., Deck, S., et al. (2009). Experimental study of shock oscillation over a transonic supercritical profile. *AIAA Journal*, 47(9), 1985–1994.

[4] Barakos, G. and Drikakis, D. (2000). Numerical simulation of transonic buffet flows using various turbulence closures. *International Journal of Heat and Fluid Flow*, 21(5), 620–626.

[5] Deck, S. (2005). Numerical simulation of transonic buffet over the OAT15A airfoil. *AIAA Journal*, 43(7), 1556–1566.

[6] Brunet, V. and Deck, S. (2008). Zonal-detached eddy simulation of transonic buffet on a civil aircraft type configuration. In *Advances in Hybrid RANS-LES Modelling*. Springer, pp. 182–191.

[7] Sartor, F. and Timme, S. (2015). Reynolds–averaged Navier–Stokes simulations of shock buffet on half wing-body configuration. *AIAA Paper 2015–1939*.

[8] Caruana, D., Mignosi, A., Corrègeand, M., et al. (2005). Buffet and buffeting control in transonic flow. *Aerospace Science and Technology*, 9(7), 605–616.

[9] Reneaux, J., Brunet, V., Caruana, D., et al. (2005). A combined experimental and numerical investigation of the buffet phenomenon and its control through passive and active devices. Tech. Rep. ONERA Tiré à Part 2005-103.

[10] Dandois, J., Molton, P., Lepage, A., et al. (2013). Buffet characterisation and control for turbulent wings. Tech. Rep. Aerospace Lab 6.

[11] Pearcey, H. H. (1961). *Shock-induced separation and its prevention by design and boundary layer control*. Pergamon.

[12] Lin, J. C. (2002). Review of research on low-profile vortex generators to control boundary-layer separation. *Progress in Aerospace Sciences*, 38(4), 389–420.

[13] Huang, J., Xiao, Z., Liu, J., et al. (2012). Simulation of shock wave buffet and its suppression on an OAT15A supercritical airfoil by IDDES. *Science China Physics, Mechanics and Astronomy*, 55(2), 260–271.

[14] Zastawny, M. (2014). Numerical simulation of wing vortex generators – methodologies and validation. In *RAeS Advanced Aero Concepts, Design and Operations Conference*.

[15] Ito, Y., Yamamoto, K., Kusunose, K., et al. (2015). Effect of vortex generators on transonic swept wings. *AIAA Paper 2015–1238*.

[16] Bender, E., Anderson, B., and Yagle, P. (1999). Vortex generator modeling for Navier–Stokes codes. In *Third ASME/JSME Joint Fluids Engineering Conference, Paper No. FEDSM99-6919*.

[17] Jirásek, A. (2005). Vortex-generator model and its application to flow control. *Journal of Aircraft*, 42(6).

[18] Dudek, J. (2011). Modeling vortex generators in a Navier–Stokes code. *AIAA Journal*, 49(4), 748–759.

[19] May, N. E. (2001). A new vortex generator model for use in complex configuration CFD solvers. *AIAA Paper 2001-31014*.

[20] Wendt, B. J. (2001). Initial circulation and peak vorticity behavior of vortices shed from airfoil vortex generators. Tech. Rep. NASA CR 2001-211144.

[21] Booker, C., Zhang, X., and Chernyshenko, S. (2009). Large-scale source term modeling of vortex generation. *AIAA Paper 2009–3951*.

[22] Peiró, J., Peraire, J., Morgan, K., et al. (1992). The numerical simulation of flow about installed aero-engine nacelles using a finite element Euler solver on unstructured meshes. *Aeronautical Journal*, (96-956).

[23] Allmaras, S. R., Johnson, F. T., and Spalart, P. R. (2012). Modifications and clarifications for the implementation of the Spalart–Allmaras turbulence model. *ICCFD7-1902*.

[24] Martineau, D. G., Stokes, S., Munday, S. J., et al. (2006). Anisotropic hybrid mesh generation for industrial RANS applications. *AIAA Paper 2006-534*.

[25] Sartor, F. and Timme, S. (2015). Mach number effects on buffeting flow on a half wing body configuration. *50th 3AF International Conference on Applied Aerodynamics*.

[26] Kay, S. M. and Marple, S. L. J. (1981). Spectrum analysis – a modern perspective. *Proceedings of the IEEE*, 69(11), 1380–1419.

[27] Burg, J. P. (1978). Maximum entropy spectral analysis. In *Modern Spectrum Analysis*. Edited by D. G. Childers, IEEE Press, New York, pp. 34–41.

COPYRIGHT STATEMENT